BBA - Bioenergetics 1866 (2025) 149512

Contents lists available at ScienceDirect

BBA - Bioenergetics

journal homepage: www.elsevier.com/locate/bbabio

# Assessment of amino acid charge states based on cryo-electron microscopy and molecular dynamics simulations of respiratory complex I

Jonathan Lasham [a,*], Amina Djurabekova [a], Georgios Kolypetris [a], Volker Zickermann [c,d], Janet Vonck [e], Vivek Sharma [a,b,*]

[a] Department of Physics, University of Helsinki, 00014 Helsinki, Finland
[b] HiLIFE Institute of Biotechnology, University of Helsinki, 00014 Helsinki, Finland
[c] Institute of Biochemistry II, University Hospital, Goethe University, 60590 Frankfurt am Main, Germany
[d] Centre for Biomolecular Magnetic Resonance, Institute for Biophysical Chemistry, Goethe University, 60438 Frankfurt am Main, Germany
[e] Department of Structural Biology, Max Planck Institute of Biophysics, 60438 Frankfurt am Main, Germany

ARTICLE INFO

*Keywords:*
Proton pump
Conformational dynamics
Electrostatics
Charge transfer
Protonation states
Coupling mechanism

ABSTRACT

The charge states of titratable amino acid residues play a key role in the function of membrane-bound bioenergetic proteins. However, determination of these charge states both through experimental and computational approaches is extremely challenging. Cryo-EM density maps can provide insights on the charge states of titratable amino acid residues. By performing classical atomistic molecular dynamics simulations on the high resolution cryo-EM structures of respiratory complex I from *Yarrowia lipolytica*, we analyze the conformational and charge states of a key acidic residue in its ND1 subunit, aspartic acid D203, which is also a mitochondrial disease mutation locus. We suggest that in the native state of respiratory complex I, D203 is negatively charged and maintains a stable hydrogen bond to a conserved arginine residue. Alternatively, upon conformational change in the turnover state of the enzyme, its sidechain attains a charge-neutral status. We discuss the implications of this analysis on the molecular mechanism of respiratory complex I.

## 1. Introduction

Bioenergetic enzymes such as photosystems and respiratory complexes catalyze charge transfer reactions by generating an electrochemical gradient across the membrane. This gradient drives the production of ATP, as was first suggested by Peter Mitchell in 1961 [1,2]. While electron transfer in the photosynthetic and respiratory complexes occurs via electron hopping or tunneling through protein-bound metal centers [3], proton transfer reactions are primarily catalyzed by hydrogen-bonded amino acid residues in conjunction with water molecules [4]. Structural and spectroscopic approaches have assisted in delineating electron transfer paths [5–9], however, proton transfer pathways are extremely difficult to characterize either by experiments or computationally [10]. One of the reasons for this is the high plasticity of hydrogen bonding networks, which depend on the charge states of titratable amino acids involved. This is further compounded by the flexibility of amino acid sidechains along with hydration/dehydration effects, resulting in proton transfer pathways being complex and multifaceted in nature.

Recent advancements in cryo-EM have led to the high resolution 3D structures of membrane proteins, with several respiratory enzyme structures solved with a resolution better than 2.5 Å [11,12]. One key advantage of cryo-EM is that the density maps can provide insights on the charge states of amino acid residues [13]. This is because the electron scattering by Coulomb potential map (cryo-EM density map) varies depending on whether the atom is charge-neutral or charged [14,15]. This allows the identification of charge states of amino acid residues in cryo-EM structures [13,16]. Broadly speaking, a lack of density for the sidechain of an acidic amino acid is reflective of its anionic state. In contrast, a clear density of its sidechain is reflective of its charge-neutral state, but in special cases, it can also be negatively charged, as discussed below.

Respiratory complex I is a large membrane protein that catalyzes redox-coupled proton translocation (Fig. 1A). The complexity of the proton pumping mechanism of complex I is markedly increased by the long-range nature of its charge transfer events. Even though there is convergence on some of the structural-mechanistic aspects, such as the presence of multiple quinone binding sites and the E channel [17], how

* Correspondence to: J. Lasham, V. Sharma, Department of Physics, University of Helsinki, 00014 Helsinki, Finland.
*E-mail addresses:* jonathan.lasham@helsinki.fi (J. Lasham), vivek.sharma@helsinki.fi (V. Sharma).

https://doi.org/10.1016/j.bbabio.2024.149512
Received 3 May 2024; Received in revised form 10 July 2024; Accepted 23 September 2024
Available online 24 September 2024

quinone reduction drives conformational and charge rearrangements to initiate proton pumping in its membrane arm still remains unclear. It is recognized that the ND1 subunit is at the heart of complex I's mechanism, coupling electron transfer in the peripheral domain to proton pumping in its membrane arm (Fig. 1A). The loop between transmembrane helices 5 and 6 and the region around it (TMH5–6 loop region), is well-recognized as one of the functionally important regions of the ND1 subunit (Fig. 1B) [18–24]. The region consists of several conserved acidic amino acid residues that are known to be important for the proton pumping function based on site-directed mutagenesis studies [23,25–27]. Significantly, some of the amino acid positions are mitochondrial disease mutant loci [28–30].

One of the strictly conserved residues, aspartic acid D203 of the ND1 subunit located in the TMH5–6 loop, has been shown - among others - to undergo conformational changes in the cryo-EM structures. Its sidechain conformation has been modeled differently in the native state of *Yarrowia lipolytica* complex I compared to the turnover state of the enzyme [23]. The native state corresponds to an enzyme prepared in the absence of substrates, whereas the turnover state corresponds to enzyme sample incubated with NADH, DBQ (decyl ubiquinone) and ubiquinol oxidase, undergoing catalysis [23]. In the structure of the native state, D203 points towards R302 of the ND1 subunit, whereas in turnover state, the sidechain points away from the arginine. Similar conformations of the two residues have been modeled in the *open/closed (active/resting)* states of mammalian complex I (Fig. S1) [31–33]. Computer simulations and photoaffinity labeling experiments have highlighted the importance of D203 in proton transfer reactions as well as in the binding of quinone analogues [34,35]. Additionally, site-directed mutagenesis experiments show D203 is critical for efficient complex I catalysis [26,27]. This efficiency is likely affected when D203 is replaced by glycine as part of a mitochondrial disease mutation [25].

By combining pKa calculations with atomistic molecular dynamics (MD) simulations of a high-resolution complex I structure, we suggested that D203 is part of a proton loading site that picks up a proton from the N side of the membrane, in response to the quinone reduction reaction, to be pumped to the P side of the membrane [23]. Accordingly, in the native state of the *Yarrowia* enzyme, D203 is likely to be in its anionic charge state, whereas in the turnover state it is charge neutral. However, a clear cryo-EM density of its sidechain observed in native complex I leads to an alternative conclusion that it may be charge-neutral in this state. Indeed, a recent high-resolution structural study of mammalian enzyme suggested that D203 is charge-neutral in the native-like conformation [31] (see also Fig. S1).

Here, we performed long time-scale atomistic unbiased MD and free energy simulations of high-resolution structures of complex I from *Yarrowia lipolytica* in different combinations of charge states to investigate D203's behavior. By analyzing the sidechain dynamics and hydrogen bonding patterns, we suggest that D203 is likely anionic in the native state of complex I, but partly charge-neutral in the turnover state. This suggests that D203 could be a part of a potential proton loading site region that responds upon quinone binding and reduction [17]. Our work highlights the power of combining structural studies with computer simulations in obtaining detailed insights into enzyme mechanism at a molecular level.

## 2. Methods

### 2.1. Atomistic Molecular Dynamics (MD) simulations and pKa calculations

All-atom unbiased molecular dynamics (MD) simulations were performed on complex I structures from *Y. lipolytica* in the native (PDB: 7O71) and turnover (PDB: 7O6Y) states [23]. The simulation setups consisted of all protein chains, a mixed lipid bilayer (50 % palmitoyl-oleoyl-phosphatidylcholine (POPC), 35 % palmitoyl-oleoyl-phosphatidylethanolamine (POPE), and 15 % cardiolipin), TIP3P water molecules and 100 mM of $Na^+/Cl^-$ ions, using the CHARMM36 forcefield [36,37]. The total system size was ~1.3 million atoms, and all minimization, equilibration and MD production steps were performed with Gromacs 2020 [38]. Full details of the simulation setup procedure can be found in previous works [23,39]. The final production simulations were performed in an NPT ensemble using the Nosé−Hoover thermostat [40,41] and Parrinello−Rahman barostat [42] at 310 K and 1 atm, respectively. Simulations were performed with the LINCS algorithm at a 2 fs timestep [43]. We used a cutoff of 12 Å for particle-mesh Ewald [44] and van der Waals interactions, with a switching distance of 10 Å. The simulation setups are listed in Table 1 (Unbiased).

The initial selection of charge states for simulations was based on pKa calculations on complex I structures in native and turnover conditions using the Propka tool [45] (setups NP and TP, respectively, see Tables 1 and S1). All aspartic acids, glutamic acids, and histidine residues were modeled as protonated if their pKa was more than 7 (Asp/Glu charge neutral and histidine with charge +1), while Lys was modeled as deprotonated (sidechain charge of zero) if its pKa was less than 7. In states NS and TS, all Asp/Glu/Lys were kept charged. Neutral His was modeled with its protonation on the δ-nitrogen in all simulations. The Propka tool was also applied on simulation snapshots to obtain the pKa of selected residues. Note, only protein atoms were considered in the pKa calculations.

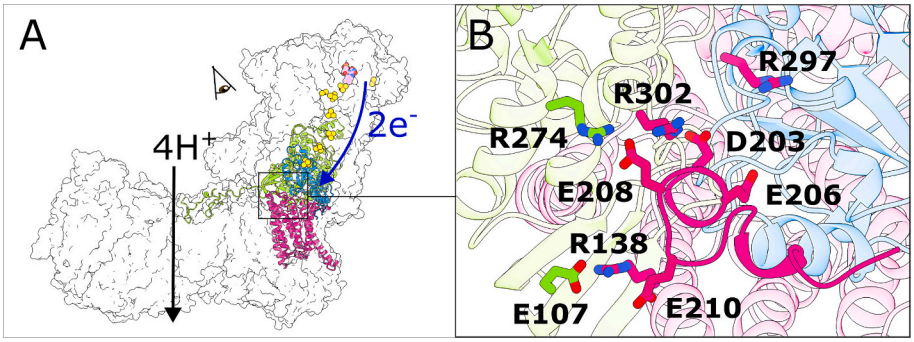


**Fig. 1.** (A) Respiratory complex I of *Yarrowia lipolytica* (PDB: 7O71) outlined with surface representation. The iron-sulphur (FeS) clusters in the hydrophilic arm of complex I are shown as spheres represented by atoms in orange (iron) and yellow (sulphur). The structurally resolved flavin mononucleotide (FMN) molecule is also shown in stick representation. The blue arrow represents the electron transfer path via FMN and FeS clusters, and the black arrow represents the transfer of four protons through the membrane arm. The three key subunits at the interface of the membrane and hydrophilic domains of complex I are represented as ribbons: ND1 in magenta, NDUFS2 in green, and NDUFS7 in blue. (B) The glutamic acids from the TMH5–6 loop in ND1 subunit are shown in stick representation together with D203. The positively charged arginine residues in the vicinity are also displayed. The colours of the subunits are as in panel A. The directional view of panel B is marked with an observer's eye in panel A. (For interpretation of the references to colour in this figure legend, the reader is referred to the web version of this article.)

**Table 1**
List of simulation setups, with the coordinates used and charge states listed.

| | Setup | Coordinates/PDB id | Charge states | Simulation lengths |
|---|---|---|---|---|
| Unbiased | NP | Native/7O71 | Propka-based | 3 × 1000 ns |
| | NS | Native/7O71 | Standard | 3 × 1000 ns |
| | TP | Turnover/7O6Y | Propka-based | 3 × 400 ns |
| | TS | Turnover/7O6Y | Standard | 3 × 400 ns |
| | NP2 | Native/7O71 | Propka-based[a] | 3 × 400 ns |
| AWH | A_NP | Native/7O71 | Propka-based | 4 × 950 ns |
| | A_NP3 | Native/7O71 | Propka-based[b] | 4 × 950 ns |
| | A_TS | Turnover/7O6Y | Propka-based | 4 × 950 ns |

Simulation replicas and lengths are listed in the last column.
[a] Charge state is calculated based on turnover/7O6Y coordinates.
[b] Charge state is calculated based on native/7O71 coordinates, but with D203 modeled charge neutral.

### 2.2. Potential of mean force (PMF) calculations using the accelerated weight histogram (AWH) method

Truncated model systems of complex I from *Y. lipolytica* consisting of subunits ND1, ND3, NDUFS2 NDUFS7 and NDUFS8 were prepared. The setup protocol described above was used and the details for the systems simulated are shown in Table 1 (AWH). First, a 4 × 200 ns unbiased MD simulation was performed for each state. The last frame of each of these simulations was used as the starting coordinates for the AWH simulation replicas, which were simulated using the multiple walker method (four walkers, Table 1, AWH) as implemented in Gromacs (*awh-multi*) [46]. The dihedral angle of D203 using atoms C-Cα-Cβ-Cγ was used as the reaction coordinate with a force constant of 1000 kJ $mol^{-1}$ $rad^{-2}$, and the defined sampling was between −180° and + 180°. Each AWH replica was run for 950 ns until the PMF plots showed minimal changes (Fig. S2).

## 3. Results and discussion

### 3.1. Protonation state of D203 based on MD simulations

Our MD simulation data show that the sidechain conformation of D203 maintains the original orientation as observed in the cryo-EM structure of native *Yarrowia* complex I when simulated in its anionic charged state (simulation setup NP, Table 1 and Fig. 2). D203 is stabilized by hydrogen bonding to conserved R302 from the ND1 subunit in the simulation of this charge state (78 % occupancy, Table 2). To test if the charge states of other residues affect the stable D203-R302 ion-pair interaction, we next analyzed MD simulations with all titratable residues modeled in their standard charged states (setup NS, Fig. 2). We find that the sidechain of D203 deviates by ~120° from the structural position with a partial loss of D203-R302 hydrogen bonding interaction (47 % occupancy, Table 2). Similarly, when the calculated charge states of the turnover structure are introduced (setup NP2), making the D203 sidechain charge-neutral, a drastic loss of D203-R302 interaction is observed (9 % occupancy, Table 2) combined with a partial change in its sidechain conformation (Fig. 2).

When the RMSF (root mean square fluctuation) of the sidechain of D203 is analyzed in these states, a similar conclusion is obtained that its sidechain shows lower fluctuations in the NP charge state compared to the NS and NP2 states (Fig. 3). Given that arginine is likely to be positively charged at neutral pH, the close interaction between the two residues, as also observed in structures [23,31–33] (Fig. S1), can be maintained if D203 is negatively charged as part of the charge state NP. Additionally, pKa calculations on MD simulation snapshots show that there is an upshift in pKa of D203 (Figs. 2 and S3) when the hydrogen bonding interaction with R302 is broken, also as part of a change in its sidechain dihedral (setup NS and NP2, see also Fig. 3).

**Table 2**
Hydrogen bond occupancies (in %) calculated from MD simulation trajectories in different charge states. Only sidechain-sidechain hydrogen bonds were considered, using a distance cut-off of 3.5 Å and an angle cut-off of 150°.

| Residue | Hydrogen bonding partner | NP | NS | TP | TS | NP2 |
|---|---|---|---|---|---|---|
| D203 | Water | 23 % | 64 % | 3 % | 18 % | 3 % |
| | R302 (ND1) | 78 % | 47 % | 26 % | 66 % | 9 % |
| | T205 (ND1) | 30 % | 50 % | 0 % | 0 % | 0 % |
| | S207 (ND1) | 10 % | 0 % | 0 % | 13 % | 0 % |
| E206 | Water | 12 % | 100 % | 3 % | 16 % | 12 % |
| | R108 (NDUFS7) | 0 % | 12 % | 0 % | 37 % | 0 % |
| E208 | Water | 16 % | 30 % | 2 % | 3 % | 15 % |
| | R274 (NDUFS2) | 25 % | 72 % | 0 % | 0 % | 17 % |
| | R302 (ND1) | 23 % | 17 % | 29 % | 0 % | 41 % |
| | S207 (ND1) | 8 % | 16 % | 0 % | 0 % | 1 % |
| E210 | Water | 0 % | 28 % | 2 % | 9 % | 12 % |
| | R138 (ND1) | 0 % | 22 % | 0 % | 33 % | 20 % |

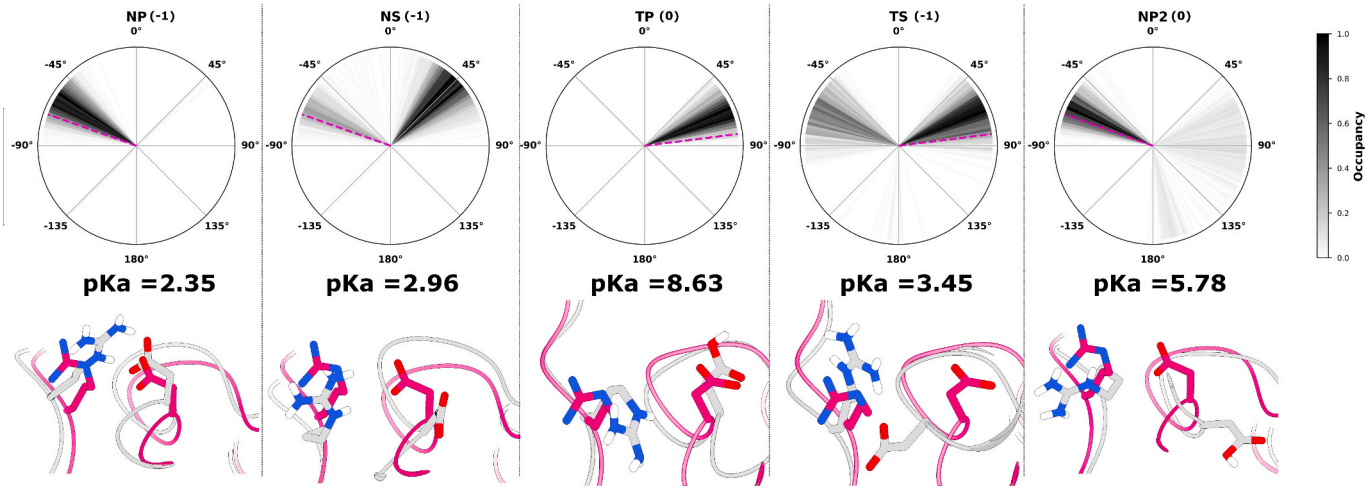


**Fig. 2.** (Top) Dihedral (C-Cα-Cβ-Cγ) of D203 in five different simulation states (see Table 1). The protonation states of D203 in each simulation are shown in brackets. The angle is plotted as a radial heatmap using 180 bins, and occupancy throughout all simulation trajectories is shown from white to black. The pink dotted line shows the starting value for the dihedral after energy minimization (see methods). (Bottom) Conformation of sidechains of D203 and R302 in *Y. lipolytica* structures (magenta) in comparison to simulation snapshots (grey). The median pKa values as calculated from MD simulation snapshots are mentioned for each setup (see Fig. S3 for the distributions).

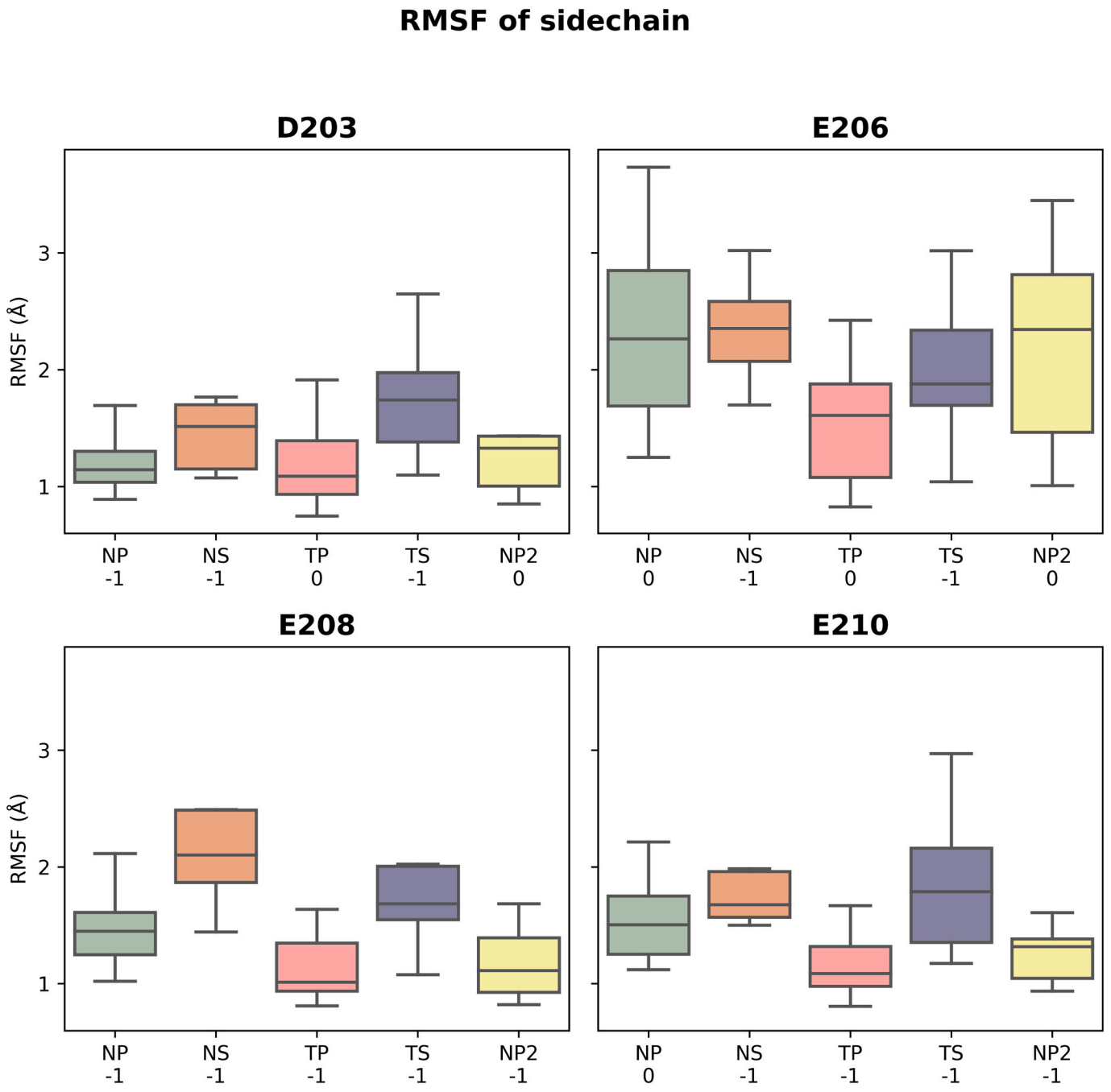


**Fig. 3.** Root-mean-squared fluctuation (RMSF) of heavy sidechain atoms in MD simulations shown as box plots. RMSF is measured from all 3 simulation replicas and combined. The charge state of the residue is shown below the setup name on the X-axis.

Interestingly, MD simulations of the turnover state of *Yarrowia* complex I show that the sidechain of D203 maintains the structural conformation when it is modeled as charge-neutral, as part of the setup TP (Fig. 2), but less so when simulated in the anionic state (setup TS, Fig. 2). The turnover state TP, with charge neutral D203, is characterized by no significant interactions involving the D203 sidechain, apart from some sporadic hydrogen bonding to R302 (26 % occupancy, Table 2), which increases to ca. 66 % when it is modeled anionic (setup TS), comparable to what is observed in the NP state. Furthermore, anionic D203 sidechain is stabilized by hydrogen bonding to water molecules, predominantly in the NS state, and less so in NP and TS states due to compensating hydrogen bonding with R302 (Table 2). However, when its sidechain is modeled neutral (NP2 and TP states), water-based hydrogen bonding is almost completely lost (Table 2). Analysis of the pKa of D203 in the TP and TS charge state simulations (Fig. S3) support the conclusion that ion-pairing between R302 and D203 considerably lowers the proton affinity of the latter residue. In contrast, a flip in the sidechain of D203 to an alternative conformation (Fig. 2) can upshift its pKa by 6–7 pK units (Fig. S3 setups NP vs TP), leading to its partial protonation.

To probe the energetics of D203 sidechain dihedral dynamics, we performed free energy simulations (see methods). The data in Fig. 4 indicate that the sidechain conformation of D203 (dihedral $\sim -50°$) is stabilized when D203 is anionic (A_NP, Table 1), whereas the second minimum (dihedral $\sim +65°$) is preferred when D203 attains the charge neutral state (A_TP and A_NP3, Table 1). This further consolidates the view that D203 is partly anionic in the native conformation, and is stabilized by R302.

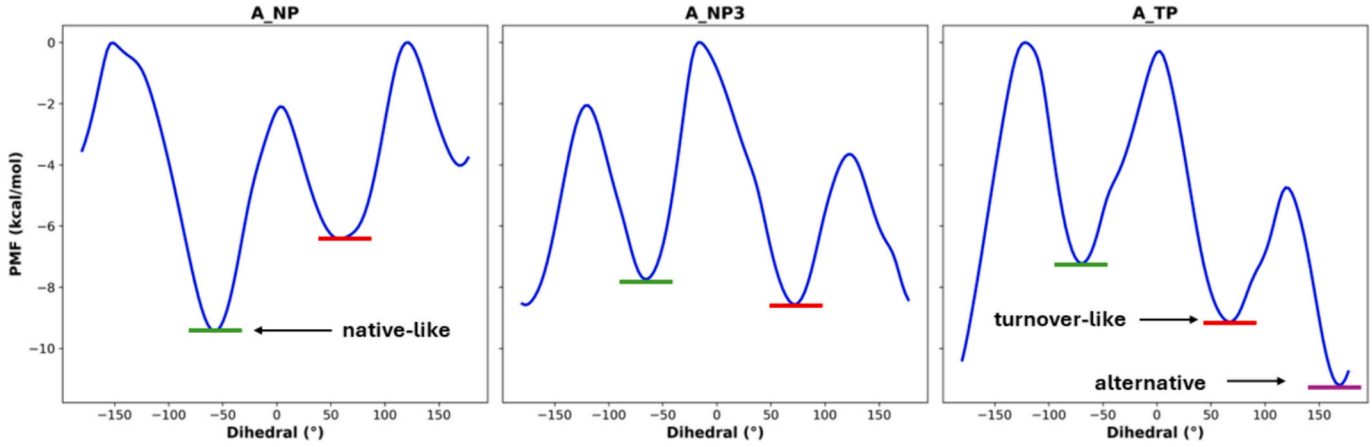


**Fig. 4.** Potential of mean force (PMF) for the rotation of the dihedral of D203 (C-Cα-Cβ-Cγ) calculated by accelerated weight histogram (AWH) method. The values were normalized by subtracting the maximum from all values.

Overall, the data point to the possibility that with the anionic sidechain and NP charge state of the enzyme, D203 maintains a relatively stable interaction with positively charged R302, as observed in the native *Yarrowia* complex I and also mammalian complexes [23,31,33]. Furthermore, the structurally observed conformation of D203 in the native state of the enzyme is not only dependent on its own charge state, but also on the charge states of the residues around it.

### 3.2. Protonation state of D203 based on cryo-EM analysis

The cryo-EM density map shows a rather clear density of the sidechain of D203 (Fig. 4A) in the native state of *Yarrowia* complex I, raising the possibility that it is charge-neutral, a notion that has indeed been considered earlier [31] (see also Section 1). However, our MD simulation data shows that if it is charge-neutral, it is less likely to maintain the hydrogen bonding interaction with R302 and its sidechain dihedral may also deviate from its structural value. Therefore, our interpretation is that the clear cryo-EM density observed for D203 in the map of native complex I state does not correspond to a neutral state of D203, but to its anionic sidechain that is stabilized in part by a positively charged R302 within hydrogen bonding distance to it.

In contrast to the clear density of D203 in the native state of the enzyme, the turnover state shows missing density (Fig. 4B), which indicates that the sidechain is either charged and/or highly mobile. A similar truncated density is observed in the cryo-EM maps of mammalian complex I [32,33]. This in turn means that the modeled sidechain conformation is likely unreliable, even though highly similar in all three structures (Fig. S1). Our MD simulation data show that the modeled conformation of D203 in *Yarrowia* complex I turnover structure can be retained with its sidechain protonated (Fig. 2), but much less so when it is anionic, where it rearranges to form a hydrogen bonding interaction with R302 akin to the native state conformation (Figs. 2, 3 and 4, Table 2). Therefore, our combined MD simulation and cryo-EM density analysis suggests that D203 in the modeled structural conformation likely corresponds to the charge-neutral state.

Overall, we conclude that D203 displays a two-state conformational dynamics model (Fig. 2). In the state when it is proximal to R302, it is predominantly anionic - a state that is stabilized in the native state of the enzyme. In the other conformation, when its sidechain points away from R302, its neutral charge state is stabilized. The loss of density of its sidechain in the turnover state is reflective not only of its higher mobility, but also of its conformation dependent pKa. These data corroborate our previous model that D203 is able to undergo conformation-coupled protonation by picking up a proton from the N side of the membrane and as part of the quinone redox chemistry can stabilize anionic quinol ($QH^-$) species (see also refs [17, 23, 47] and Section 3.4).

### 3.3. Dynamics of the TMH5-6 loop

We next analyzed the protonation-dependent conformational dynamics of the three conserved glutamic acid residues (E206, E208 and E210) on the same TMH5–6 loop, but downstream from D203. In addition to D203, the three residues are also found to undergo conformational rearrangements in the native and turnover states of *Y. lipolytica* complex I [23] and influence the dynamics of D203 (see Section 3.1). Our pKa calculations on the high-resolution structures suggest that E206 is charge-neutral in both the native and the turnover states of complex I [23]. However, in simulations of both the structures, the neutral sidechain of E206 is found to be much more mobile in comparison to the states when it is modeled anionic (Fig. 3). Analysis of cryo-EM density maps of both native and turnover states show truncated density, suggesting the charged nature of the sidechain (Fig. 5). Due to the lack of clear density, the atomic model of its sidechain is unreliable. In our recent work, we remodeled its sidechain to an alternative conformation [39], which also lowered its proton affinity in agreement with the cryo-EM density analysis that it is likely to be anionic. Our analysis indicates that E206 is in part anionic in both the native and turnover states of *Yarrowia* complex I, and the negatively charged sidechain is stabilized by hydrogen bonds with water molecules as well as with the conserved R108 from NDUFS7 (Table 2), a residue that is known to affect complex I catalysis and Q dynamics [48] (see also Fig. 5).

Based on the pKa calculations, we find that E208 is charged in both the native and turnover structures of *Yarrowia* complex I. In the MD simulations of the native state (setup NP), lower fluctuations of the sidechain are observed (Fig. 3) in contrast to when all titratable residues are modeled in their charged states (setup NS). The sidechain conformation is also maintained closer to the modeled state (Fig. S4). The native-like arrangement of E208 side chain (setup NP) is characterized by ion pairing with conserved arginine residues (R274/25 %; R302/23 %, Table 2). Our cryo-EM density analysis also suggests that E208 is likely charged in the native conformation as well as in the turnover state (Fig. 5), and therefore the modeled sidechain in both structures should be considered approximate. Interestingly, the MD simulations of turnover state TP show a major deviation of the sidechain from the modeled structural conformation, consistent in all simulation replicas (Fig. S4). This alternate position is extremely stable (Fig. 3) and is likely due to an electrostatic interaction forming with R302, which becomes more available to form an ion pair due to D203 being neutral in this state. Therefore, in line with the structural analysis, our MD simulations suggest that E208 is likely anionic also in the turnover state of the enzyme.

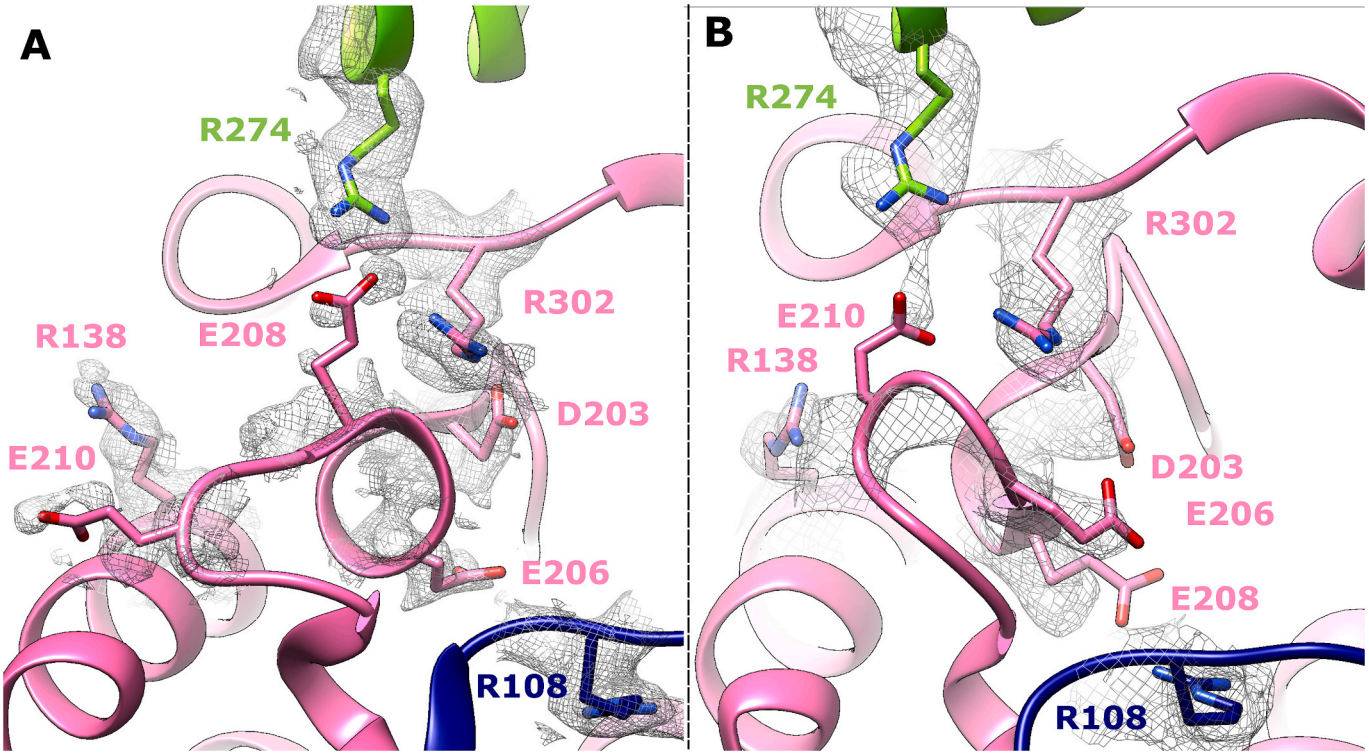


**Fig. 5.** The glutamic acids from the TMH5–6 loop in the ND1 subunit are shown together with R138, D203 and R302 in stick representation, with the cryo-EM density overlayed. Also shown are R108 from NDUFS7 (blue) and R274 from NDUFS2 (green). (A) shows native complex I (PDB 7O71, EMD-12742) and (B) complex I under turnover (PDB 7O6Y, EMD-12741). (For interpretation of the references to colour in this figure legend, the reader is referred to the web version of this article.)

Finally, we examined E210, which is modeled as neutral in the native but charged in the turnover state of complex I based on pKa analysis on native and turnover structures of *Yarrowia* complex I. In both the native and turnover state MD simulations, the sidechain conformation matches relatively well with the structures (Fig. S4), and the stability of the sidechains is higher than in the NS and TS simulations where all Lys/Asp/Glu are modeled charged (Fig. 3). Intriguingly, when analyzing the interactions in the NP and TP simulations, no significant ion pairs or hydrogen bonds were identified. This is despite the turnover structure showing a possible ion pair to R302. In the simulations, this ion pair does not form, likely due to competition with E208 and D203. Cryo-EM analysis of this residue suggests a weaker density of its sidechain in the native than in the turnover state and suggests that it is likely charged in both the states but is partly stabilized by positively charged R302 in the latter state.

Overall, these data lead us to suggest that E206, E208, and E210 are all likely to be negatively charged in both the native and turnover states, and that they compete for ion pairing with the same positively charged residues as D203, thereby affecting the conformational dynamics of the TMH5–6 loop as a whole. We also find that D203 displays a two-state scenario, where each state can be characterized by a unique combination of charge and conformation. We note that the conventional MD simulations and free energy approaches applied here do not allow change in protonation state on the fly, instead rapidly developing constant pH simulation methods would be necessary to achieve exhaustive coupled conformational and protonation state sampling [49,50].

### 3.4. Mechanistic implications

Analysis of the atomic models of complex I show D203 from the ND1 subunit is in close proximity to the conserved R302 of the same subunit (Fig. S1). For instance, the approximate distance between the two residues is 4–5 Å in *Yarrowia* native complex I [23], whereas the sidechains are modeled much closer in the resting (active) state of complex I from mouse [31]. Given the region is relatively well-resolved in the cryo-EM maps of these two structures, one can expect higher accuracy of the modeled sidechains. However, protonation states of these residues remain difficult to assign based on structural coordinates. Our simulation data supports the viewpoint that D203 is likely anionic in the native/resting state of complex I, achieved by the stabilization of hydrogen bonding to R302. In contrast, in the turnover state of the *Yarrowia* enzyme, it can attain a rotated sidechain conformation stabilized by the protonation of its sidechain. This suggests that D203 is part of the proton loading site region of complex I that picks up a proton from the N side of the membrane, which will eventually be pumped to the P side of the membrane, as part of the quinone binding and reduction mechanism [17,23]. The proton from the N phase may arrive from the pathways that originate at E39 of the ND3 subunit or E107 of the NDUFS2 subunit, as discussed in [17] (see also [51]).

It should be noted that even though residue R302 is highly conserved, mutation to alanine in *E. coli* complex I does not significantly affect the Q reductase activity [26]. This in part dilutes its role of stabilizing the anionic state of D203. However, scrutinizing sequence alignments [52] and structural data of *E. coli* complex I show that a histidine (H210, *E. coli* complex I numbering) resides near D203 (D213 in *E. coli* complex I numbering) [11], which can take up the role of arginine in its absence. It is important to emphasize that respiratory complex I is a robust enzyme, and probably has several fail-safe mechanisms against single amino acid exchanges.

The TMH5–6 loop, which consists of the four strictly conserved acidic residues discussed here, resides at the interface of the hydrophilic and membrane domains of complex I, and undergoes structural rearrangements, suggesting it is at the heart of the coupling between electron transfer to quinone and proton pumping in the membrane domain. The structural rearrangement of the TMH5–6 loop from native to turnover conditions involves the movement of these acidic residues, bringing

E208, E206 and D203 in close proximity to one another [23]. This conformational transition is likely to bring a change in the pKa of these acidic residues. Our simulation data and analysis of cryo-EM density suggest that E206, E208 and E210 can remain anionic in both the native and turnover states of complex I, whereas D203 undergoes conformation-dependent protonation reactions commensurate with its proton-loading site function [17,23].

## CRediT authorship contribution statement

**Jonathan Lasham:** Writing – review & editing, Writing – original draft, Visualization, Investigation, Formal analysis, Data curation, Conceptualization, Methodology. **Amina Djurabekova:** Writing – review & editing, Visualization, Investigation, Formal analysis, Data curation, Conceptualization, Methodology. **Georgios Kolypetris:** Investigation, Data curation. **Volker Zickermann:** Writing – review & editing, Validation, Methodology, Funding acquisition, Formal analysis, Conceptualization. **Janet Vonck:** Writing – review & editing, Visualization, Investigation, Formal analysis, Conceptualization. **Vivek Sharma:** Writing – original draft, Supervision, Resources, Project administration, Investigation, Funding acquisition, Conceptualization, Methodology.

## Declaration of competing interest

The authors declare that they have no known competing financial interests or personal relationships that could have appeared to influence the work reported in this paper.

## Data availability

Data will be made available on request.

## Acknowledgements

VS acknowledges research funding from the Academy of Finland, the Jane and Aatos Erkko Foundation, the Sigrid Jusélius Foundation, the Magnus Ehrnrooth Foundation, the Cancer Foundation, Finland and the Faculty of Science (University of Helsinki). JV and VZ were supported by the German Research Foundation (CRC 1507 – Membrane-associated Protein Assemblies, Machineries, and Supercomplexes; P14). High-performance computing resources from the Center for Scientific Computing, Finland are acknowledged. We are also thankful to the HiLIFE internship programme and the IT support of the Faculty of Science, University of Helsinki. VS thanks Gerrit Groenhof for helpful discussion on the AWH method. JL acknowledges travel grant support from the Finnish Society of Sciences and Letters.

## Appendix A. Supplementary data

Supplementary data to this article can be found online at https://doi.org/10.1016/j.bbabio.2024.149512.

## References

[1] P. Mitchell, Coupling of phosphorylation to electron and hydrogen transfer by a chemi-osmotic type of mechanism, Nature 191 (4784) (1961) 144–148.
[2] M. Wikström, C. Pecorilla, V. Sharma, Chapter two - the mitochondrial respiratory chain, in: L.S. Kaguni, F. Tamanoi (Eds.), The Enzymes, Academic Press, 2023, pp. 15–36.
[3] C.C. Moser, T.A. Farid, S.E. Chobot, P.L. Dutton, Electron tunneling chains of mitochondria, Biochim. Biophys. Acta (BBA)-Bioenerg. 1757 (9) (2006) 1096–1109.
[4] H. Ishikita, K. Saito, Proton transfer reactions and hydrogen-bond networks in protein environments, J. R. Soc. Interface 11 (91) (2014) 20130518.
[5] L.A. Sazanov, P. Hinchliffe, Structure of the hydrophilic domain of respiratory complex I from *Thermus thermophilus*, Science 311 (5766) (2006) 1430–1436.
[6] C. Hunte, V. Zickermann, U. Brandt, Functional modules and structural basis of conformational coupling in mitochondrial complex I, Science 329 (5990) (2010) 448–451.
[7] M.L. Verkhovskaya, N. Belevich, L. Euro, M. Wikström, M.I. Verkhovsky, Real-time electron transfer in respiratory complex I, Proc. Natl. Acad. Sci. 105 (10) (2008) 3763–3767.
[8] L. Euro, D.A. Bloch, M. Wikström, M.I. Verkhovsky, M. Verkhovskaya, Electrostatic interactions between FeS clusters in NADH: ubiquinone oxidoreductase (Complex I) from *Escherichia coli*, Biochemistry 47 (10) (2008) 3185–3193.
[9] H.R. Bridges, E. Bill, J. Hirst, Mössbauer spectroscopy on respiratory Complex I: the iron–sulfur cluster ensemble in the NADH-reduced enzyme is partially oxidized, Biochemistry 51 (1) (2012) 149–158.
[10] É. Bertalan, A.-N. Bondar, Graphs of protein-water hydrogen bond networks to dissect structural movies of ion-transfer microbial rhodopsins, Front. Chem. 10 (2023).
[11] V. Kravchuk, O. Petrova, D. Kampjut, A. Wojciechowska-Bason, Z. Breese, L. Sazanov, A universal coupling mechanism of respiratory complex I, Nature 609 (2022) 1–7.
[12] F. Kolbe, S. Safarian, Ż. Piórek, S. Welsch, H. Müller, H. Michel, Cryo-EM structures of intermediates suggest an alternative catalytic reaction cycle for cytochrome c oxidase, Nat. Commun. 12 (1) (2021) 6903.
[13] M.A. Marques, M.D. Purdy, M. Yeager, CryoEM maps are full of potential, Curr. Opin. Struct. Biol. 58 (2019) 214–223.
[14] W. Kühlbrandt, D.N. Wang, Y. Fujiyoshi, Atomic model of plant light-harvesting complex by electron crystallography, Nature 367 (6464) (1994) 614–621.
[15] J. Wang, On the appearance of carboxylates in electrostatic potential maps, Protein Sci. 26 (3) (2017) 396–402.
[16] S. Maki-Yonekura, K. Kawakami, K. Takaba, T. Hamaguchi, K. Yonekura, Measurement of charges and chemical bonding in a cryo-EM structure, Commun. Chem. 6 (1) (2023) 98.
[17] A. Djurabekova, J. Lasham, O. Zdorevskyi, V. Zickermann, V. Sharma, Long-range electron proton coupling in respiratory complex I—insights from molecular simulations of the quinone chamber and antiporter-like subunits, Biochem. J. 481 (7) (2024) 499–514.
[18] J. Zhu, K.R. Vinothkumar, J. Hirst, Structure of mammalian respiratory complex I, Nature 536 (7616) (2016) 354–358.
[19] D.N. Grba, J. Hirst, Mitochondrial complex I structure reveals ordered water molecules for catalysis and proton translocation, Nat. Struct. Mol. Biol. 27 (10) (2020) 892–900.
[20] X. Pan, D. Cao, F. Xie, F. Xu, X. Su, H. Mi, X. Zhang, M. Li, Structural basis for electron transport mechanism of complex I-like photosynthetic NAD(P)H dehydrogenase, Nat. Commun. 11 (1) (2020) 1–11.
[21] T. Masuya, S. Uno, M. Murai, H. Miyoshi, Pinpoint dual chemical cross-linking explores the structural dynamics of the ubiquinone reaction site in mitochondrial complex I, Biochemistry 60 (10) (2021) 813–824.
[22] E. Laube, J. Meier-Credo, J.D. Langer, W. Kühlbrandt, Conformational changes in mitochondrial complex I of the thermophilic eukaryote *Chaetomium thermophilum*, Sci. Adv. 8 (47) (2022) eadc9952.
[23] K. Parey, J. Lasham, D.J. Mills, A. Djurabekova, O. Haapanen, E.G. Yoga, H. Xie, W. Kühlbrandt, V. Sharma, J. Vonck, High-resolution structure and dynamics of mitochondrial complex I—insights into the proton pumping mechanism, Sci. Adv. 7 (46) (2021) eabj3221.
[24] O. Haapanen, M. Reidelbach, V. Sharma, Coupling of quinone dynamics to proton pumping in respiratory complex I, Biochim. Biophys. Acta (BBA)-Bioenerg. 1861 (12) (2020) 148287.
[25] F. Nuber, J. Schimpf, J.-P. Di Rago, D. Tribouillard-Tanvier, V. Procaccio, M.-L. Martin-Negrier, A. Trimouille, O. Biner, C. von Ballmoos, T. Friedrich, Biochemical consequences of two clinically relevant ND-gene mutations in *Escherichia coli* respiratory complex I, Sci. Rep. 11 (1) (2021) 12641.
[26] P.K. Sinha, J. Torres-Bacete, E. Nakamaru-Ogiso, N. Castro-Guerrero, A. Matsuno-Yagi, T. Yagi, Critical roles of subunit NuoH (ND1) in the assembly of peripheral subunits with the membrane domain of *Escherichia coli* NDH-1, J. Biol. Chem. 284 (15) (2009) 9814–9823.
[27] M. Kervinen, R. Hinttala, H.M. Helander, S. Kurki, J. Uusimaa, M. Finel, K. Majamaa, I.E. Hassinen, The MELAS mutations 3946 and 3949 perturb the critical structure in a conserved loop of the ND1 subunit of mitochondrial complex I, Hum. Mol. Genet. 15 (17) (2006) 2543–2552.
[28] O. Musumeci, A.L. Andreu, S. Shanske, N. Bresolin, G.P. Comi, R. Rothstein, E. A. Schon, S. DiMauro, Intragenic inversion of mtDNA: a new type of pathogenic mutation in a patient with mitochondrial myopathy, Am. J. Hum. Genet. 66 (6) (2000) 1900–1904.
[29] E.L. Blakely, K.J. Rennie, L. Jones, M. Elstner, Z.M.A. Chrzanowska-Lightowlers, C. B. White, J.P.H. Shield, D.T. Pilz, D.M. Turnbull, J. Poulton, R.W. Taylor, Sporadic intragenic inversion of the mitochondrial DNA MTND1 gene causing fatal infantile lactic acidosis, Pediatr. Res. 59 (3) (2006) 440–444.
[30] E. Pronicka, D. Piekutowska-Abramczuk, E. Ciara, J. Trubicka, D. Rokicki, A. Karkucińska-Więckowska, M. Pajdowska, E. Jurkiewicz, P. Halat, J. Kosińska, A. Pollak, M. Rydzanicz, P. Stawinski, M. Pronicki, M. Krajewska-Walasek, R. Płoski, New perspective in diagnostics of mitochondrial disorders: two years' experience with whole-exome sequencing at a national paediatric centre, J. Transl. Med. 14 (1) (2016) 174.
[31] D.N. Grba, I. Chung, H.R. Bridges, A.-N.A. Agip, J. Hirst, Investigation of hydrated channels and proton pathways in a high-resolution cryo-EM structure of mammalian complex I, Sci. Adv. 9 (31) (2023) eadi1359.

[32] A.-N.A. Agip, J.N. Blaza, H.R. Bridges, C. Viscomi, S. Rawson, S.P. Muench, J. Hirst, Cryo-EM structures of complex I from mouse heart mitochondria in two biochemically defined states, Nat. Struct. Mol. Biol. 25 (7) (2018) 548–556.
[33] D. Kampjut, L.A. Sazanov, The coupling mechanism of mammalian respiratory complex I, Science 370 (6516) (2020).
[34] V. Sharma, G. Belevich, A.P. Gamiz-Hernandez, T. Róg, I. Vattulainen, M. L. Verkhovskaya, M. Wikström, G. Hummer, V.R.I. Kaila, Redox-induced activation of the proton pump in the respiratory complex I, Proc. Natl. Acad. Sci. 112 (37) (2015) 11571–11576.
[35] M. Murai, Y. Mashimo, J. Hirst, H. Miyoshi, Exploring interactions between the 49 kDa and ND1 subunits in mitochondrial NADH-ubiquinone oxidoreductase (complex I) by photoaffinity labeling, Biochemistry 50 (32) (2011) 6901–6908.
[36] A.D. MacKerell Jr., D. Bashford, M. Bellott, R.L. Dunbrack Jr., J.D. Evanseck, M. J. Field, S. Fischer, J. Gao, H. Guo, S. Ha, All-atom empirical potential for molecular modeling and dynamics studies of proteins, J. Phys. Chem. B 102 (18) (1998) 3586–3616.
[37] J.B. Klauda, R.M. Venable, J.A. Freites, J.W. O'Connor, D.J. Tobias, C. Mondragon-Ramirez, I. Vorobyov, A.D. MacKerell Jr., R.W. Pastor, Update of the CHARMM all-atom additive force field for lipids: validation on six lipid types, J. Phys. Chem. B 114 (23) (2010) 7830–7843.
[38] M.J. Abraham, T. Murtola, R. Schulz, S. Páll, J.C. Smith, B. Hess, E. Lindahl, GROMACS: high performance molecular simulations through multi-level parallelism from laptops to supercomputers, SoftwareX 1 (2015) 19–25.
[39] J. Lasham, A. Djurabekova, V. Zickermann, J. Vonck, V. Sharma, Role of protonation states in the stability of molecular dynamics simulations of high-resolution membrane protein structures, J. Phys. Chem. B 128 (10) (2024) 2304–2316.
[40] S. Nosé, A unified formulation of the constant temperature molecular dynamics methods, J. Chem. Phys. 81 (1) (1984) 511–519.
[41] W.G. Hoover, Canonical dynamics: equilibrium phase-space distributions, Phys. Rev. A 31 (3) (1985) 1695–1697.
[42] M. Parrinello, A. Rahman, Polymorphic transitions in single crystals: a new molecular dynamics method, J. Appl. Phys. 52 (12) (1981) 7182–7190.
[43] B. Hess, P-LINCS: a parallel linear constraint solver for molecular simulation, J. Chem. Theory Comput. 4 (1) (2008) 116–122.
[44] T. Darden, D. York, L. Pedersen, Particle mesh Ewald: an N·log(N) method for Ewald sums in large systems, J. Chem. Phys. 98 (12) (1993) 10089–10092.
[45] M.H. Olsson, C.R. Søndergaard, M. Rostkowski, J.H. Jensen, PROPKA3: consistent treatment of internal and surface residues in empirical pKa predictions, J. Chem. Theory Comput. 7 (2) (2011) 525–537.
[46] V. Lindahl, J. Lidmar, B. Hess, Accelerated weight histogram method for exploring free energy landscapes, J. Chem. Phys. 141 (4) (2014) 044110.
[47] F. Nuber, L. Mérono, S. Oppermann, J. Schimpf, D. Wohlwend, T. Friedrich, A quinol anion as catalytic intermediate coupling proton translocation with electron transfer in *E. coli* respiratory complex I, Front. Chem. 9 (2021) 291.
[48] E. Galemou-Yoga, O. Haapanen, I. Wittig, K. Siegmund, V. Sharma, V. Zickermann, Mutations in a Conserved Loop in the PSST Subunit of Respiratory Complex I Affect Ubiquinone Binding and Dynamics, Biochim. Biophys. Acta (BBA)-Bioenerg. 1860 (7) (2019) 573–581.
[49] V. Martins de Oliveira, R. Liu, J. Shen, Constant pH molecular dynamics simulations: current status and recent applications, Curr. Opin. Struct. Biol. 77 (2022) 102498.
[50] P. Buslaev, N. Aho, A. Jansen, P. Bauer, B. Hess, G. Groenhof, Best practices in constant pH MD simulations: accuracy and sampling, J. Chem. Theory Comput. 18 (10) (2022) 6134–6147.
[51] E. Galemou Yoga, K. Parey, A. Djurabekova, O. Haapanen, K. Siegmund, K. Zwicker, V. Sharma, V. Zickermann, H. Angerer, Essential role of accessory subunit LYRM6 in the mechanism of mitochondrial complex I, Nat. Commun. 11 (1) (2020) 6008.
[52] J. Warnau, V. Sharma, A.P. Gamiz-Hernandez, A. Di Luca, O. Haapanen, I. Vattulainen, M. Wikström, G. Hummer, V.R.I. Kaila, Redox-coupled quinone dynamics in the respiratory complex I, Proc. Natl. Acad. Sci. 115 (36) (2018) E8413–E8420.